Received: 24 May 2024 | Revised: 10 September 2024 | Accepted: 10 October 2024

DOI: 10.1002/psp4.13262

ARTICLE

Local depletion of large molecule drugs due to target binding in tissue interstitial space

Tatiana Zasedateleva[1] | **Stephan Schaller**[1] | **Elizabeth C. M. de Lange**[2] | **Wilhelmus E. A. de Witte**[1]

[1]ESQlabs GmbH, Saterland, Germany

[2]Division of Systems Pharmacology and Pharmacy, Leiden Academic Centre for Drug Research, Leiden University, Leiden, The Netherlands

Correspondence
Wilhelmus E. A. de Witte, ESQlabs GmbH, Am Sportplatz 7, Saterland 26683, Germany.
Email: wilbert.dewitte@esqlabs.com

Abstract

Drug–target binding determines a drug's pharmacodynamics but can also have a profound impact on a drug's pharmacokinetics, known as target-mediated drug disposition (TMDD). TMDD models describe the influence of drug–target binding and target turnover on unbound drug concentrations and are frequently used for biologics and drugs with nonlinear plasma pharmacokinetics. For drug targets expressed in tissues, the effect of TMDD may not be detected when analyzing plasma concentration curves, but it might still affect tissue concentrations and occupancy. This review aimed to investigate the likeliness of such a scenario by reviewing the literature for a typical range of TMDD parameter values and their impact on local drug concentrations and target occupancy in a whole-body PBPK model with TMDD. Our analysis demonstrated that tissue drug concentrations are impacted and significantly depleted in many physiological scenarios. In contrast, the effect on plasma concentrations is much lower, specifically for smaller organs with lower perfusion. Moreover, in scenarios with fast internalization of the drug–target complex, the distribution of large molecules from plasma to tissue interstitial space emerges as a rate-limiting step for the drug–target interaction. These factors may lead to overpredicting local drug concentrations when considering only plasma pharmacokinetics. A sensitivity analysis revealed the high and not always intuitive impact of drug-specific parameters, including the drug molecule hydrodynamic radius, dissociation constant (K_d), drug–target complex internalization rate constant (k_{int}), and target dissociation rate constant (k_{off}), on the drug's pharmacokinetics. Our analysis demonstrated that tissue TMDD needs to be considered even if plasma pharmacokinetics are linear.

Study Highlights

WHAT IS THE CURRENT KNOWLEDGE ON THE TOPIC?

Minimal mechanistic TMDD models with target binding in plasma or in a peripheral compartment have been explored extensively and are well understood.

However, the combined effect of slow, size-dependent tissue distribution as described by the two-pore model and TMDD due to target binding in tissue has been described much less and is not well understood.

WHAT QUESTION DID THIS STUDY ADDRESS?

How likely is it for a large molecule that TMDD plays a significant role in the tissue concentrations when target binding occurs only in the interstitial space of the target organ?

WHAT DOES THIS STUDY ADD TO OUR KNOWLEDGE?

Local drug depletion due to target mediated clearance is likely to occur in many drug development scenarios for biologics. This phenomenon is often not reflected by nonlinear plasma concentration profiles.

HOW MIGHT THIS CHANGE DRUG DISCOVERY, DEVELOPMENT, AND/OR THERAPEUTICS?

Model-based prediction of drug concentrations and target engagement should include the rate of drug distribution and the target turnover. Target turnover and target concentrations should be measured more routinely for biologics.

INTRODUCTION

In the traditional depiction of drug action, a drug dose leads to a certain concentration profile in plasma and the site of action, where drug–target binding leads to the initiation of the drug effect, meaning that pharmacokinetics influences pharmacodynamics and not vice versa. In fact, this principle applies in many cases when the target expression is low relative to drug concentration, the target turnover rate is slow compared with the drug half-life, the drug–target binding is reversible and short due to low drug affinity and non-specific off-target binding outweighs the effects of on-target tissue binding on the drug's pharmacokinetic profile. Nevertheless, in certain cases where these listed prerequisites are not met, drug–target binding can influence the drug concentrations at the site of action. While this phenomenon can be relevant to both small and large molecules, it often has a more significant impact on the pharmacokinetics of large molecules, and this review will focus specifically on large molecules.

In 1994, Levy introduced the term target-mediated drug disposition (TMDD)[1] to describe the scenario where drug–target binding significantly affects the (local) drug concentrations. While Levy, in his original publication, focused on the tissue retention driven by target binding of small molecules in target-expressing tissues, TMDD was soon extended to include target turnover and increased plasma clearance, especially for large molecules.[2–5] For large molecules, the role of target and drug–target complex internalization is especially relevant due to their high specificity to the target, strong target binding affinity, and often long plasma half-lives in the absence of target binding.[6–8] The TMDD equations and model behavior have been studied extensively, which has led to several ways to simplify the model and reduce the number of parameters,[2] as well as to an understanding of the most critical parameters and parameter combinations, such as the ratio of affinity and target concentration that drives the maximal fraction of the drug bound to the target and the product of drug–target complex internalization and the target concentration that drives the maximal rate of elimination of the bound drug.[4,9]

Drug–target binding often occurs in tissues rather than in plasma.[10] For small molecules, the distribution from plasma to interstitial space can be considered too fast to become the rate-limiting step. For large molecules, fast internalization of the drug–target complex might cause the distribution from plasma to tissue interstitial space to be rate-limiting for the drug–target interaction.[11] Moreover, such localized target-mediated clearance might have a limited impact on plasma concentrations compared with interstitial concentrations, depending on the size and distribution kinetics of the tissue where the target is expressed. Therefore, conventional TMDD investigations that consider plasma concentrations solely when assessing a drug's pharmacokinetics can overpredict the actual drug concentration at the target site. This can result in incorrect dosage regimens and affect therapy effectiveness. The potential for localized TMDD and its implication renders typical TMDD parameters, such as the target concentration and target turnover, relevant for many drug development and clinical scenarios, even if nonlinear pharmacokinetics are not observed in plasma. However, these key parameters are often unknown and difficult to obtain in the early stages of drug development projects.[7,11,12]

The limited impact of target binding in tissues on plasma concentrations and the lack of well-defined reference values for TMDD parameters in tissue–target

binding pose challenges in drug discovery and development. In this study, we aimed to get a broad overview of physiological values from the literature for the general target-related TMDD parameters: the target concentration, the target degradation rate constant (k_{deg}), and the drug–target complex internalization rate constant. We also aimed to identify the likelihood of local TMDD for large molecule drugs, whose target is expressed in the tissue, using the typical parameter values. In addition, we aimed to generate a comprehensive understanding of the rate-limiting steps for drug–target interactions in tissue interstitial space.

In our study, we used a TMDD model integrated with a whole-body PBPK model. The whole-body PBPK part allows a convenient and flexible exploration of many scenarios with a target expressed in any main organ(s), in different species, and for drug molecules with different molecular sizes without structural model adjustments. This makes a whole-body PBPK model advantageous compared with minimal PBPK models, where the target organ is typically represented as a separate compartment that needs an independent parameterization and where a modification in the structure would be required in case of target binding in multiple organs.

METHODS

Typical ranges of target-related TMDD parameters

An extensive literature review was conducted to gather reference values for target concentration, target degradation, target synthesis (k_{syn}), and drug–target complex internalization rate constants. Most of the k_{syn} values were calculated as the target concentration multiplied by the k_{deg}, assuming target concentrations are a result of steady-state with target synthesis and target degradation.

The collected data were categorized with respect to several characteristics. The source of each parameter value was a model-based estimation, an in vivo measurement, or an ex vivo/in vitro measurement. In addition, the values were categorized based on the species, organs, or compartments for the model estimates, and the prevalent localizations of the targets in the body. We included targets expressed in the membrane of tissue cells, in the membrane of blood cells, targets that are expressed intracellularly, and soluble targets.

After retrieving the parameter values from the available literature, the 25th, 50th, and 75th percentiles were calculated for each parameter. From these values, we defined the typical ranges for simulation by rounding the 25th and 75th percentiles to the nearest order of magnitude that encompasses these ranges.

To avoid bias in the calculated ranges by the number of concentration measurements for each target (Figure S1), the medians were calculated for each target separately, after which the desired statistics were derived from these values. For the remaining parameters, such as k_{deg}, k_{int}, and k_{int}/k_{deg} ratio, where there were not many values for each specific target, we computed medians from all available data without segmenting them into target groups.

Software

All simulations were performed in Rstudio Version 2023.3.0.386 coupled to R version 4.2.2, using esqlabsR v5.1.1.9000 and ospsuite-R v12.0.0 packages. We utilized a whole-body Physiologically Based Pharmacokinetic model (PK-Sim v11.0).[13]

Model and equations

In the model, the membrane-bound target was expressed in the heart or muscle interstitial space, and the drug was simulated as a large molecule in the large molecule model.[14] This model describes the distribution and clearance of large molecules based on their distribution kinetics and recirculation from the interstitial space of the organs to the venous blood via lymph flow, as defined by the two-pore formalism. Additionally, it includes mechanisms such as endosomal clearance of molecules after their pinocytotic uptake and FcRn-mediated salvage from the endosomes by recycling of FcRn-bound molecules back to plasma or interstitial space.

The free target amount, free drug interstitial amount, and drug–target complex amount were described by the following equations:

$$\frac{dT}{dt} = k_{syn} - k_{deg} * T - k_{on} * D * \frac{T}{V_T} + k_{off} * DT$$

$$\frac{dD}{dt} = k_{off} * DT - k_{on} * D * \frac{T}{V_T}$$

$$\frac{dDT}{dt} = k_{on} * D * \frac{T}{V_T} - k_{off} * DT - k_{int} * DT$$

where T refers to the target amount, D represents the drug amount in tissue, DT indicates the drug–target complex amount, k_{syn} is the zero-order target synthesis rate constant, k_{deg} is the first-order target degradation rate constant, k_{on} is the second-order drug–target association rate constant, k_{off} is the first-order drug–target dissociation rate constant, k_{int}

is the first-order drug–target complex internalization rate constant, and V_T is the tissue interstitial volume.

In the drug–target complex internalization reaction, k_{int} was implemented indirectly as k_{deg} multiplied by the k_{int}/k_{deg} ratio (Supporting Information S1).

Simulations

From the literature review, the typical ranges of values for each parameter were determined based on the corresponding 25th and 75th percentiles for interstitial targets in humans. These interstitial targets encompass only soluble targets and those expressed in the membranes of tissue cells. Targets expressed in the membrane of blood cells and intracellular targets were not included in the calculation.

To evaluate the impact of target concentration and target turnover, we ran 16 scenarios with the membrane-bound target expressed either in the heart or muscle. Each scenario corresponded to one combination of the target concentration and degradation rate constant values, where values were defined based on physiological ranges with steps of 10-fold. Notably, the target concentrations we employed represented concentrations for the entire organs, and the software automatically recalculated the interstitial concentrations by dividing the whole organ concentration by the volume fraction of interstitial space of the organ (0.1 in muscle and 0.16 in heart).

During the simulation exercise, the drug-specific properties were fixed to the values indicated in Table 1, while the target-specific parameter values varied within scenarios. The drug was administered as an intravenous bolus at a dose of 1 mg/kg, and the simulations were conducted for single and repeated drug administration with a frequency of once every 2 weeks.

After the simulations with constant drug-specific parameters, the drug-specific parameters were included in a sensitivity analysis, which was repeated for all the target-specific scenarios.

TABLE 1 Drug-specific parameter values defined for the initial model simulations.

Parameter	Value
FcRn affinity in endosomes	0.75 μM
FcRn affinity in plasma	999 999 μM
Unbound fraction in plasma	1
Molecular weight	150 kDa
Hydrodynamic radius	5.13e−3 μm
k_{off}	1 h^{-1}
K_d	1 nM
k_{int}/k_{deg} ratio	0.1
Dose	1 mg/kg

Repeated sensitivity analysis

In the local sensitivity analysis, we investigated the impact of the K_d, k_{off}, k_{int}, and drug molecule hydrodynamic radius. The parameters were varied relative to the values in Table 1. This sensitivity analysis was repeated for all the scenarios, for single and repeated dosing.

To assess the effect of k_{int}, we varied the value of the k_{int}/k_{deg} ratio since k_{deg} was fixed in the scenarios. The ranges of variation in the sensitivity analysis for the drug-specific parameters k_{int}/k_{deg} ratio, k_{off}, and K_d covered a span from a 1000-fold decrease to a 1000-fold increase in reference values in increments of 10 to cover the wide range of potential drug properties in the drug discovery space. For the k_{int}/k_{deg} ratio, this range was specifically chosen to incorporate all possible k_{int} values within the respective span across all scenarios.

The variation range for the hydrodynamic radius of the drug molecule was different and composed of the following values: ⅓, ½, ⅗, ⅘, 1, 1⅕, 1⅖, 2, 3. This range was chosen to encompass a diverse set of molecule sizes, ranging from single-domain nanobodies and full-length antibodies to larger entities such as IgA complexes.

To determine the driving factors for the results of the sensitivity analysis, we conducted a causal chain normalization using the formula:

$$\text{Normalized sensitivity} = \frac{\text{sensitivity effect (\% of reference)}}{\text{sensitivity cause (\% of reference)}}$$

For this normalization, a unidirectional causal chain was assumed from the drug's plasma concentration to its interstitial concentration and target occupancy.

RESULTS

Typical ranges of target-related TMDD parameters

We conducted a thorough literature review to gather the currently available data on a wide range of targets. The complete tables with all the collected values of target concentrations, synthesis, degradation, and internalization rate constants, and calculated k_{int}/k_{deg} ratios can be found in Supporting Information S2.[10,15–91] In addition to these values, the supplemental tables contain information about species, methods of estimation, localizations of the targets, references to the corresponding literature sources,

and some other case-specific details that could be of help to researchers.

The most abundant dataset was compiled for target concentration, encompassing values for 49 distinct targets. For some targets, multiple values of this parameter were obtained (Figure S1) from different studies, species, or organs. The most frequently occurring organ in the target concentration data was the brain, but the distribution of target concentration in the brain did not appear to differ much from the other organs (Figure S2).

General ranges

From the collected dataset, realistic ranges were calculated, which were applied as limits to our simulations and sensitivity analyses. The 25th, 50th, and 75th percentiles for each relevant parameter were computed using only the interstitially expressed target values from human studies. Although the model developed mostly applies to membrane-bound targets, we included both tissue membrane-bound and soluble targets in the range calculation to retain as much data as possible and limit the exclusion of potentially relevant scenarios (Figure S3).

In order to reflect the uncertainty that comes with the collected dataset, its limited number of data points, and its heterogeneity, we used the order of magnitude that encompasses the interquartile range as the limit for the realistic simulation scenarios. The resulting values are presented in Table 2. The range column provides the range to the nearest order of magnitude that includes the interquartile range.

Difference between species

The observed differences in the target-related parameters between species are limited compared with the variability within each species, and most of the interquartile ranges overlap, as shown in Figure S4. While this reduces the significance of interspecies differences, a few trends were observed.

The comparison across different species shows a similar distribution of target concentration values, with a median of ~10 nM. It should be noted that the degradation rate constants are generally higher than internalization rate constants for all included species, with the entire interquartile range of the k_{int}/k_{deg} ratio below 1, except for rats, where the dataset is the smallest. Additionally, the most significant interspecies difference is obtained for the k_{int}, which tends to be lower in humans and monkeys than in mice and rats, in line with the generally increased metabolic rates in lower body weight species.

Difference between soluble and membrane-bound targets

The data collected showed that soluble targets typically exhibit lower concentrations than targets expressed in tissue cell membranes and intracellularly (Figure 1). As for kinetic constants, the degradation rate constant tends to be higher for soluble targets, while membrane-bound targets expressed in tissues show higher internalization rates, and therefore, a higher k_{int}/k_{deg} ratio. Remarkably, almost all k_{int}/k_{deg} ratio values are lower than 1 for soluble targets, while they are distributed around 1 for membrane targets.

Simulations with the target expressed in the heart

We investigated 16 scenarios with different target-specific parameter values that are within the range identified by the literature review, for both single and repeated dosing. No substantial difference was observed for plasma concentrations, interstitial concentrations, or target occupancy between single and repeated dosing simulations. Many of the simulated scenarios demonstrated local depletion of the drug, as indicated by the strongly decreasing interstitial concentrations with increasing target concentrations and turnover, while plasma concentrations were hardly affected (Figure 2).

To assess whether TMDD parameters have a comparable effect on the drug's pharmacokinetics across different organs expressing the target, we conducted simulations for two organs with distinct characteristics: heart and muscle.

Parameter	25%	50%	75%	Range
Target concentration, nM	0.17	1.49	13.1	0.1–100
k_{deg}, h^{-1}	0.029	0.21	1.39	0.01–10
k_{int}, h^{-1}	0.0044	0.026	0.17	0.001–1
k_{int}/k_{deg} ratio	0.095	0.19	0.75	0.01–1

TABLE 2 Summary statistics and typical ranges for target concentration, k_{deg}, k_{int}, and k_{int}/k_{deg} ratio.

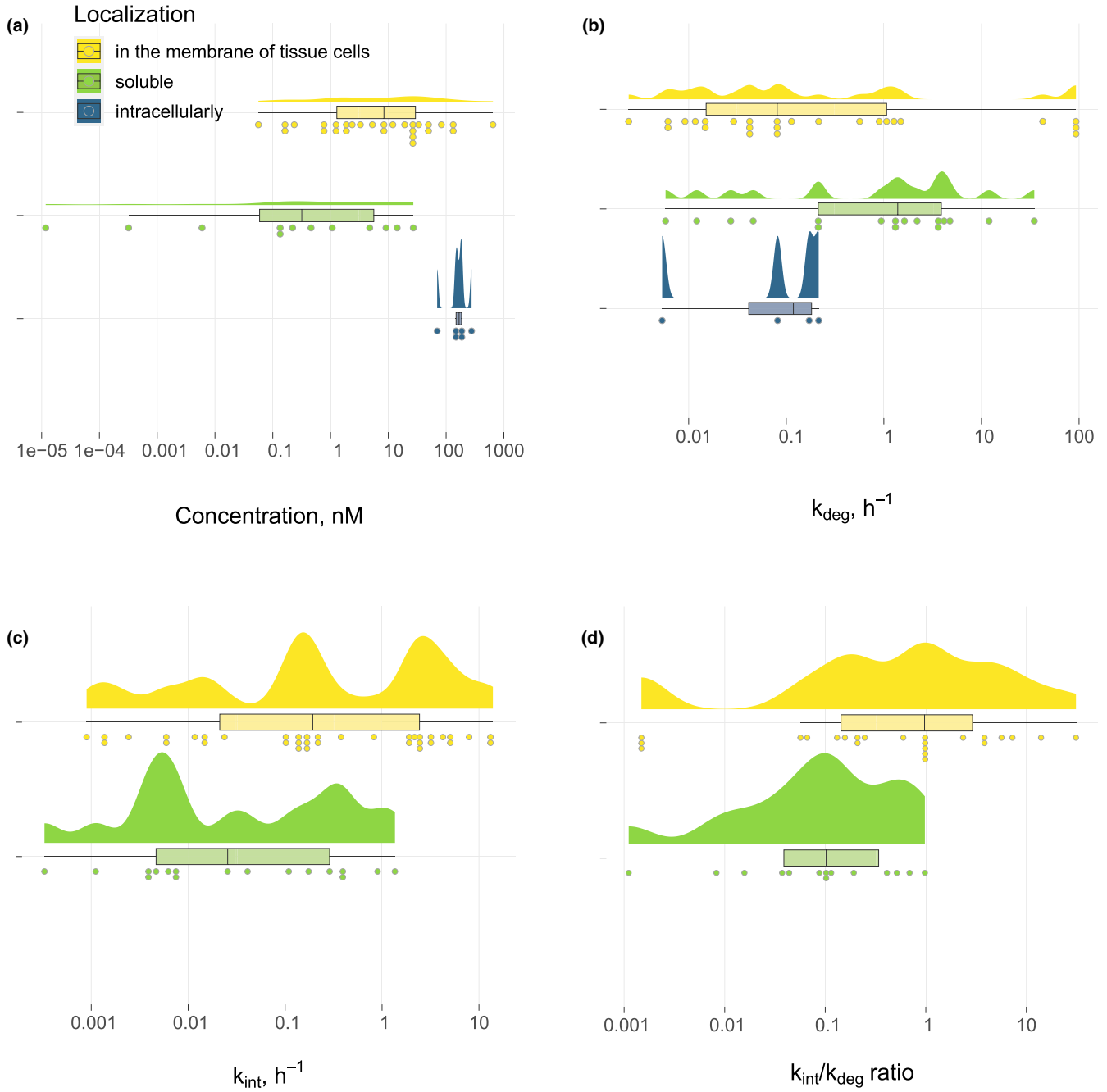

FIGURE 1 Distribution of target concentration, k_{deg}, k_{int}, and k_{int}/k_{deg} ratio by target localization. The data from all species was included. The data for the concentration graph was grouped by the target name, with each dot representing the median for a specific target. Shaded areas represent density distributions, dots represent individual data points, and boxplots indicate the three quartiles with whiskers extending up to 1.5 * IQR (Inter Quartile Range, that is, from the 25th to the 75th percentiles).

The heart, a relatively small organ, has a volume of 0.42 liters in our human model. The simulations revealed that TMDD parameters affect the concentration–time profile of a drug in the interstitial space of the heart (Figure 2). In systems where target turnover is higher, the concentration of free drug molecules in the tissue is lower, and the impact of target turnover increases as the target concentration rises. Consequently, combinations of TMDD parameters resulting in faster clearance lead to the depletion of the drug in the interstitial space.

Despite the apparent impact of the TMDD parameters on the local drug concentration, this effect is not evident in the plasma drug concentrations (Figure 2).

Simulations with the target expressed in muscle

Conversely to the heart, muscle, the largest organ in the human PBPK model (32.64 L in the default human model),

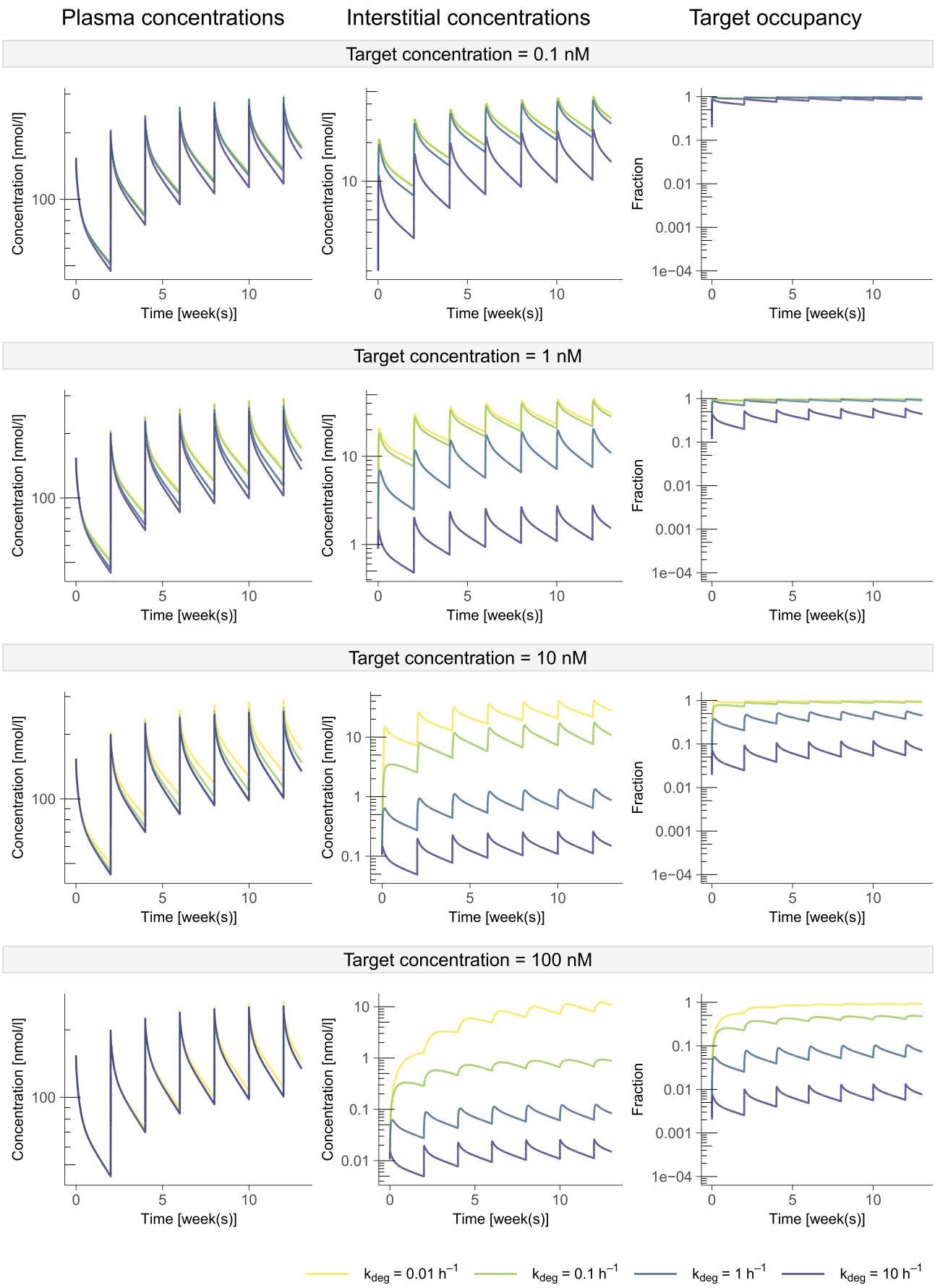

FIGURE 2 Comparative simulations of plasma concentrations, interstitial concentrations, and target occupancy with a large molecule PBPK—TMDD model for a target that is expressed in the heart interstitial space. Constant parameter values are given in Table 1.

exhibits a more extensive distribution with respect to the amount of a drug from the blood to the tissue than the heart, although distribution to the muscle is slower. The same simulations as performed for a target expressed in the heart demonstrated a noteworthy effect of TMDD parameters on the concentration of the drug in plasma for a target expressed in muscle (Figure S5). However, even with the target expressed in muscle, the impact of TMDD in the interstitial space on plasma concentrations is limited to ~1 order of magnitude on trough concentrations, and increasing the target concentration or k_{deg} has no further impact beyond this point. The impact on interstitial concentrations does not reach such a limit and goes up to four orders of magnitude on trough concentrations.

Another remarkable aspect lies in the absence of the classical nonlinear pattern in plasma curves, even when the plasma clearance is affected by local TMDD due to the high tissue volume of the muscle.

Sensitivity analysis

We conducted an extensive repeated sensitivity analysis to assess the impact of various drug-specific parameters on key pharmacokinetic parameters, drug concentrations, and target occupancy. Our investigation encompassed several drug-specific parameters: hydrodynamic radius of the drug molecule, K_d, k_{off}, and k_{int}. For each parameter of the molecule, we examined broad ranges that cover most drug discovery scenarios. The sensitivity analysis was repeated for all target-specific scenarios simulated in the previous section. While some results were consistent between heart and muscle, others diverged. The results for single and repeated dosing scenarios did not represent a crucial difference.

Sensitivity analysis for the hydrodynamic radius

The hydrodynamic radius was the only parameter significantly affecting the drug's plasma concentrations (Figure 3). The effect was more remarkable in the simulations with the target expressed in the muscle, particularly in the 1.71–5.13e−3 μm range (data not shown), which corresponds to the molecular weight of ~10–150 kDa. This range encompasses various molecules, spanning from relatively small nanobodies (~15 kDa) to larger entities such as full-length antibodies (150 kDa).

The sensitivity analysis for the hydrodynamic radius shows a significant and inverse impact of small molecular size on the AUC and more extensively on the drug concentration at the end of the simulation (C_tEnd) in scenarios where the product of target concentration and degradation rate constant is the highest. This combination of parameter values leads to an increased target-mediated clearance in the tissues, and a faster distribution to the tissues increases the impact of tissue clearance on plasma concentrations. It is important to highlight that in this sensitivity analysis exercise, only one parameter was changed at a time. Therefore, the results cannot be directly applied to predict target occupancy for nanobodies, for example, which lack affinity for the FcRn receptor and can have significant renal clearance.

Sensitivity analysis for K_d

The changes in K_d showed considerable influence on the interstitial drug concentration. A 100-fold change in K_d from the reference value leads to a 100-fold change in summary parameters for interstitial concentrations in extreme cases (Figure 4). Increasing the K_d (i.e., reducing the affinity) results in decreasing target binding and target-mediated clearance, and thus, higher concentrations of free drug in tissue if the distribution to the tissue is rate-limiting. However, a decreased drug affinity does not increase the occupancy as the increase in interstitial concentrations is proportional to the decrease in equilibrium binding, and in the end, the affinity does not affect the occupancy under the condition with fast local drug clearance (Figures 4 and 6). It should be noted here that a change in K_d is applied with constant k_{off} and is effectively a change in k_{on} in our model parameterization.

Sensitivity analysis for k_{off}

To understand the sensitivity analysis results for the k_{off} (Figure 4), it is essential to note that when k_{off} is changed, k_{on} is also changed with the same factor, as the K_d remains constant. Furthermore, in a TMDD model, the receptor occupancy with constant drug concentrations is determined by the steady-state constant K_{ss} rather than the K_d, with $K_{ss} = (k_{off} + k_{int})/k_{on}$. This means that for scenarios where the k_{off} is much smaller than the k_{int}, a decrease in k_{off} and k_{on} increases the K_{ss}.

The k_{off} has a similar but inverse impact as the K_d on one-half of the sensitivity plot (Figure 4). When k_{off} is much lower than k_{int}, the k_{off} dramatically affects the drug interstitial concentration. The k_{off} value of 0.001 h^{-1} is associated with a significantly higher drug concentration in comparison with a reference value of 1 h^{-1}.

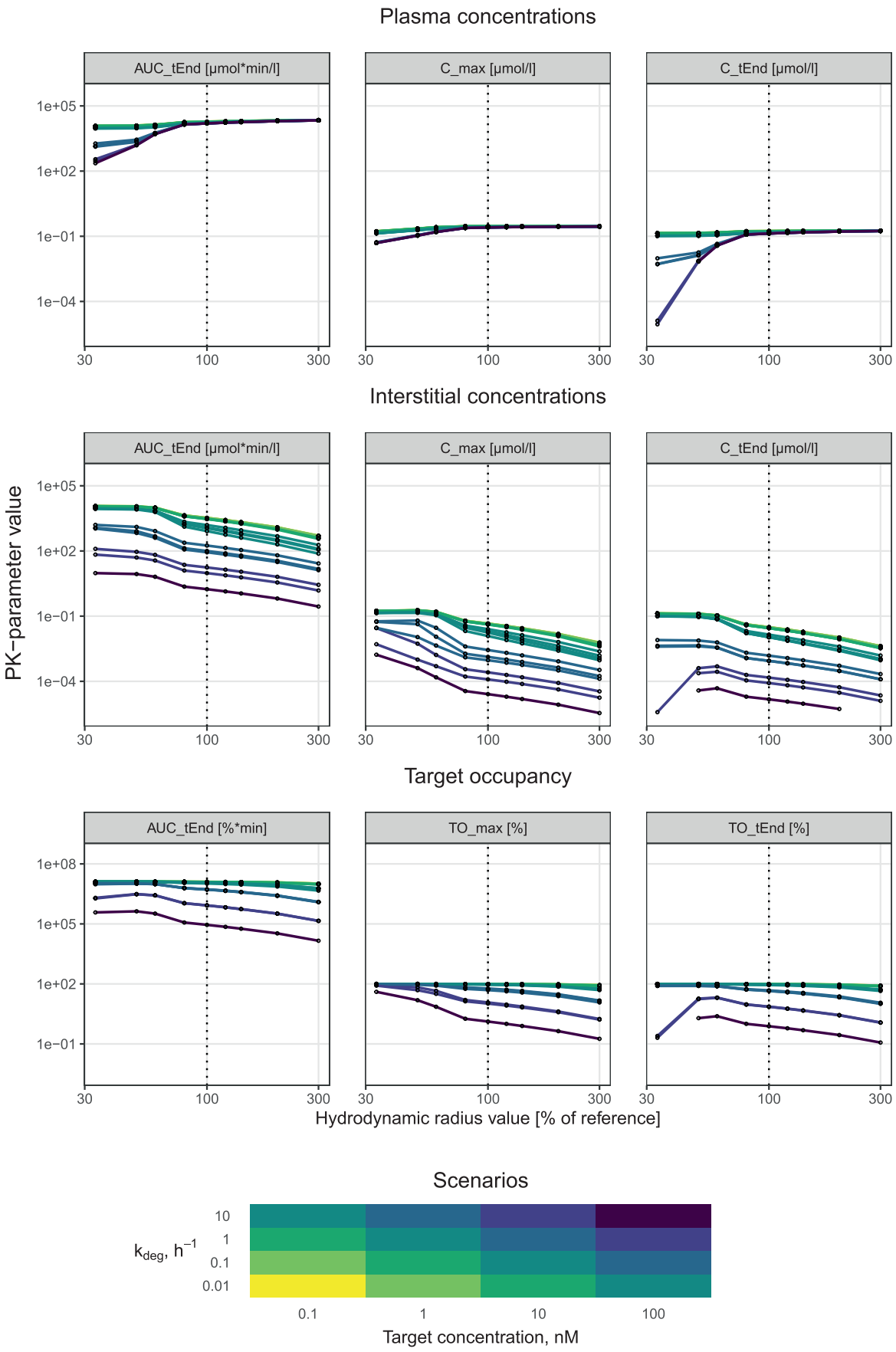

FIGURE 3 Sensitivity spider plots for the hydrodynamic radius for its impact on plasma concentrations, interstitial concentrations, and target occupancy when the target is expressed in the heart. The reference value is 5.13e−3 µm.

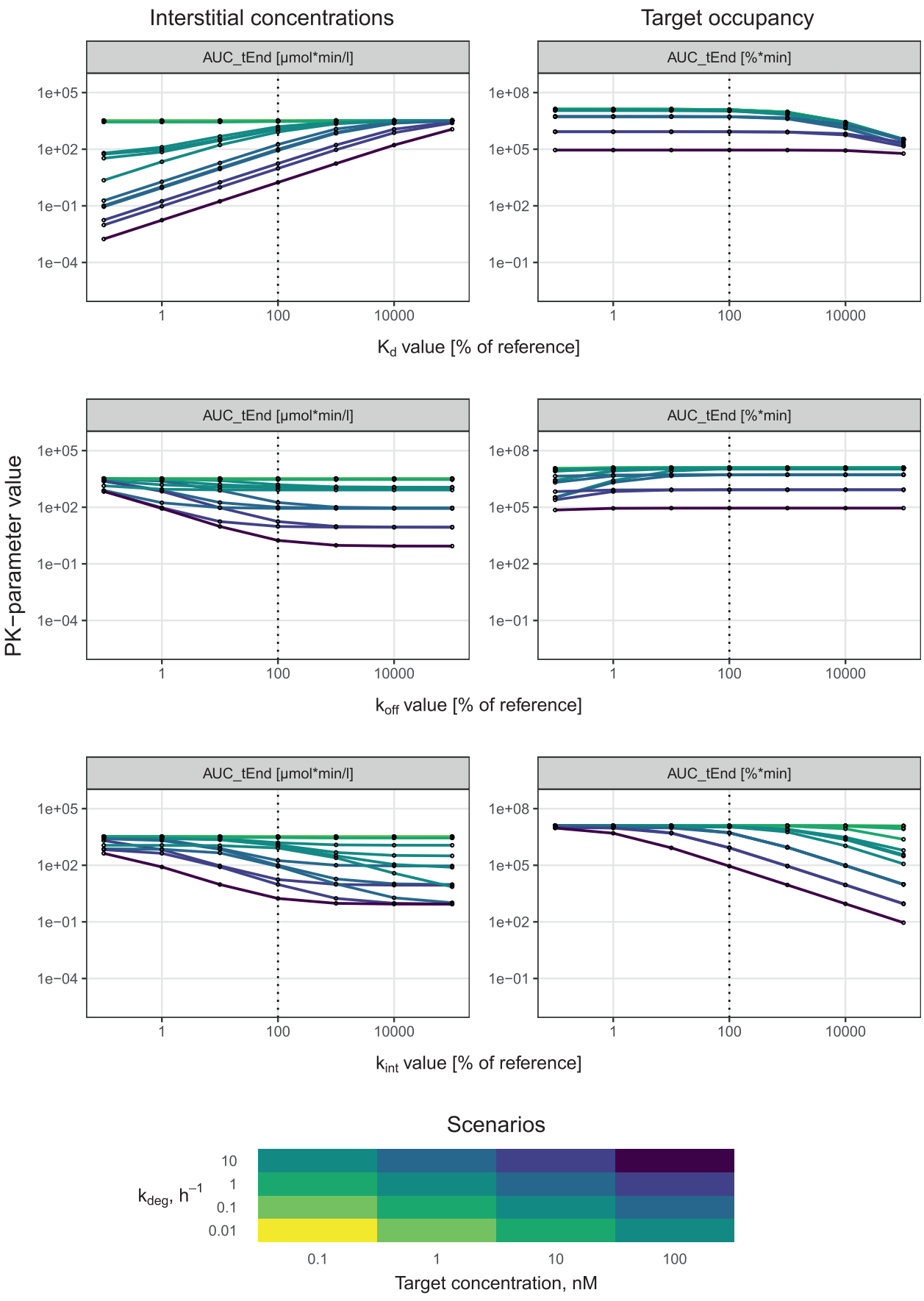

FIGURE 4 Sensitivity spider plots for the K_d, k_{off}, and k_{int} for their impacts on interstitial concentrations and target occupancy when the target is expressed in the heart. The reference values are 1 nM, 1 $h^{-1}$and 0.1 (k_{int}/k_{deg} ratio), respectively.

Sensitivity analysis for k_{int}

The sensitivity analysis demonstrated a pronounced effect of the k_{int} value on the drug concentration in tissue and target occupancy (Figure 4). A higher rate of drug–target complex internalization leads to faster local drug depletion and lower target occupancy. The extent of this effect correlates with the product of target concentration and degradation rate constant.

DISCUSSION

This review aimed to evaluate the relevance of TMDD of interstitially expressed membrane targets in a single target organ, with heart and muscle as example target organs. This was done firstly by reviewing the available literature to provide the relevant ranges for the target-related parameters that determine the extent and kinetics of TMDD. Subsequently, we explored the impact of each of those parameters for a typical antibody with the identified parameter ranges and evaluated how this impact was dependent on drug-specific properties in a repeated local sensitivity analysis. We found that local concentration depletion is likely to happen for a drug exhibiting local TMDD.

The relevant target-related TMDD parameters for this investigation included the target concentration, degradation of the unbound target (k_{deg}), and degradation of the drug–target complex (k_{int}).

Target-related TMDD parameter ranges

We gathered information on target concentration, synthesis, degradation, internalization rate constants, and the k_{int}/k_{deg} ratio for a variety of drug targets (Supporting Information S2). The collected literature data revealed some valuable information with respect to target-related parameter values. Firstly, the interquartile ranges of target concentrations and their turnovers for membrane targets are limited to two orders of magnitude (Figure 1), which provides a good starting point in the absence of observed data for a specific project or for our generic simulation study. Secondly, the difference in parameter values between species (Figure S4) and between target types are limited, relative to the variability and considering the small sample size. A clear difference appears for intracellular targets, which all seem to have relatively high concentrations in comparison with membrane targets and soluble targets, which have the lowest concentrations.

In addition, the data showed that the k_{int}/k_{deg} ratio is lower than 1 with a median around 0.1 for almost all the presented soluble targets but not for membrane-bound ones, with a median around 1 (Figure 1). The k_{int}/k_{deg} ratio <1 suggests that in general, drug–target binding protects the target from degradation. This could be explained by the size increase that can limit the renal filtration upon binding of the soluble target to a large molecule drug.

Simulations with varying target-specific parameter values

The simulated scenarios demonstrated that for a typical antibody size (150 kDa), the combination of target turnover and target concentration parameter values from our literature study leads to local TMDD and depletion of interstitial drug concentrations in most simulated scenarios. However, if target binding happens only in a relatively small organ, the local depletion of the interstitial drug concentrations is not reflected in the plasma concentration profile. Therefore, in such a case, the actual influence of TMDD parameters would be hardly detectable through conventional blood concentration measurements. To investigate such a scenario, target expression in the heart, which has one of the fastest distribution kinetics rates among the "non-leaky" tissues, comparable to the "leaky" tissues, spleen, kidneys, and liver, was taken as an example in this research. The results were contrasted with target expression in the muscle, which has a much larger volume.

When the drug–target interaction occurs in muscle, changes in the extent of local TMDD are more reflected in the plasma concentrations, as the higher volume of this organ leads to more extensive distribution from plasma to muscle in terms of amounts (Figure S5).

Moreover, the classical sigmoidal/nonlinear pattern is not observed in plasma curves, even in scenarios where the drug–target interaction affects the plasma concentrations (data not shown). This underscores once again the importance of paying attention to the interstitial drug concentration profile when the drug's membrane target is expressed within the tissue. Such an approach becomes essential in providing accurate recommendations for optimal drug dosing strategies and dose selections in (first-in-human) clinical study design. For example, in the simulated scenario in Figure 2 for a target concentration of 1 nM and a degradation rate constant of $10\,h^{-1}$, the simulated dose would not be sufficient to achieve continuous occupancy >50%, and an increase in the dose of about 10-fold would be required to achieve such a threshold.

To facilitate a deeper understanding of the modeled system, we provide a Tissue TMDD shiny app incorporating the developed model. This interactive tool provides an intuitive platform for exploring and analyzing the system.

Sensitivity analysis for drug-specific parameters

The scenario simulations showed that the distribution from plasma to the tissue interstitial space is likely to become the rate-limiting step on the causal path from drug dosing to target-mediated elimination for an interstitially expressed membrane target. In the situation with the most extensive target-mediated clearance, this becomes a unidirectional process where virtually all the drug that enters the tissue is bound to the target and gets degraded, and virtually no drug returns from interstitial space to plasma (Figure 5). The sensitivity analysis allowed us to characterize the impact of drug molecules' hydrodynamic radius, k_{off}, K_d, and k_{int} on the drug concentration in the interstitial space and plasma and on the target occupancy. These four parameters are the drug-specific parameters that determine the critical processes on the causal path from drug dosing to target-mediated elimination. One should note that this study investigates the impact of isolated drug-specific properties on multiple TMDD-related system-specific properties, but combined changes of multiple drug-specific properties are not taken into account. For example, most biologic molecules with a decreased hydrodynamic radius compared with monoclonal antibodies are subject to increased renal clearance, which dramatically shortens their pharmacokinetic half-lives, but in our sensitivity analysis, only the hydrodynamic radius was changed to investigate the impact of this parameter in isolation.

Identifying a predominant causal chain, as depicted in Figure 5, is a useful framework to aid in the interpretation of the sometimes non-intuitive results of the repeated sensitivity analysis. For example, decreasing the hydrodynamic radius of a large molecule increases the distribution to the tissue interstitial space and would, therefore, increase tissue concentrations and occupancy. However, decreasing the solute's hydrodynamic radius also increases the drug's clearance from plasma via the target-mediated pathway in the tissue, which translates into lower tissue concentrations. To shed more light on these opposing impacts, we can use the identified causal chain and normalize the sensitivity of one output for the sensitivity of the previous step in the causal chain. We can, for example, normalize the sensitivity of the interstitial drug concentration to the hydrodynamic radius for the sensitivity of the plasma concentrations (Figure 6) and reveal the isolated impact of the hydrodynamic radius on the interstitial concentrations relative to the plasma concentrations.

The parameters characterizing the formation of the drug–target complex also had a non-intuitive impact on our simulations. An increase in the K_d value (i.e., a decrease in affinity) normally leads to a reduced occupancy with constant drug concentration. However, in the case of extensive local TMDD, it also increases the interstitial concentration, as less drug is internalized via the target binding. These two effects happen to the extent that they cancel out each other's impact and that the affinity does not impact the occupancy in the condition with rate-limiting plasma-tissue distribution (see Figure 4). However, normalization of the sensitivity of target occupancy by the sensitivity of tissue concentration allows us to take into account changes in interstitial concentration, and it becomes evident that target occupancy is sensitive to changes in the drug's affinity in all scenarios, even with fast local TMDD clearance (Figure 6).

To interpret the findings of the sensitivity analysis for the k_{off} (Figure 4), it is essential to take into account that changes in k_{off} also mean similar changes in k_{on} due to a constant K_d value, as k_{on} is defined in our model as k_{off}/K_d. Moreover, in a TMDD model, the steady-state constant K_{ss}, determined as $K_{ss}=(k_{off}+k_{int})/k_{on}$, is more relevant than the K_d and determines the receptor occupancy with constant drug concentrations.[2] This implies that in cases when k_{off} is considerably smaller than k_{int}, a decrease in both k_{off} and k_{on} leads to an increase in K_{ss}. For the lowest extreme of the sensitivity analysis, where the k_{off} is 1% of the reference value of $1\,h^{-1}=0.01\,h^{-1}$, the k_{off} is smaller than or equal to the k_{int} for ¾ of the scenarios, whereas at the highest extreme, the k_{off} is larger than the k_{int} for all scenarios. All of this means that there is no impact of the k_{off} on the K_{ss} on the right side of the sensitivity analysis, and given the lack of sensitivity for increased k_{off} values, that the binding kinetics do not have a significant impact between a k_{off} of 1 and $100\,h^{-1}$. Considering that the left side of the sensitivity analysis for k_{off} mirrors the right

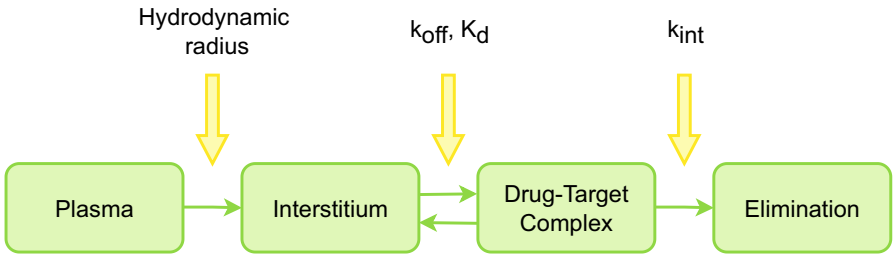

FIGURE 5 Influence of model parameters on various stages of a drug's fate within the context of extensive TMDD.

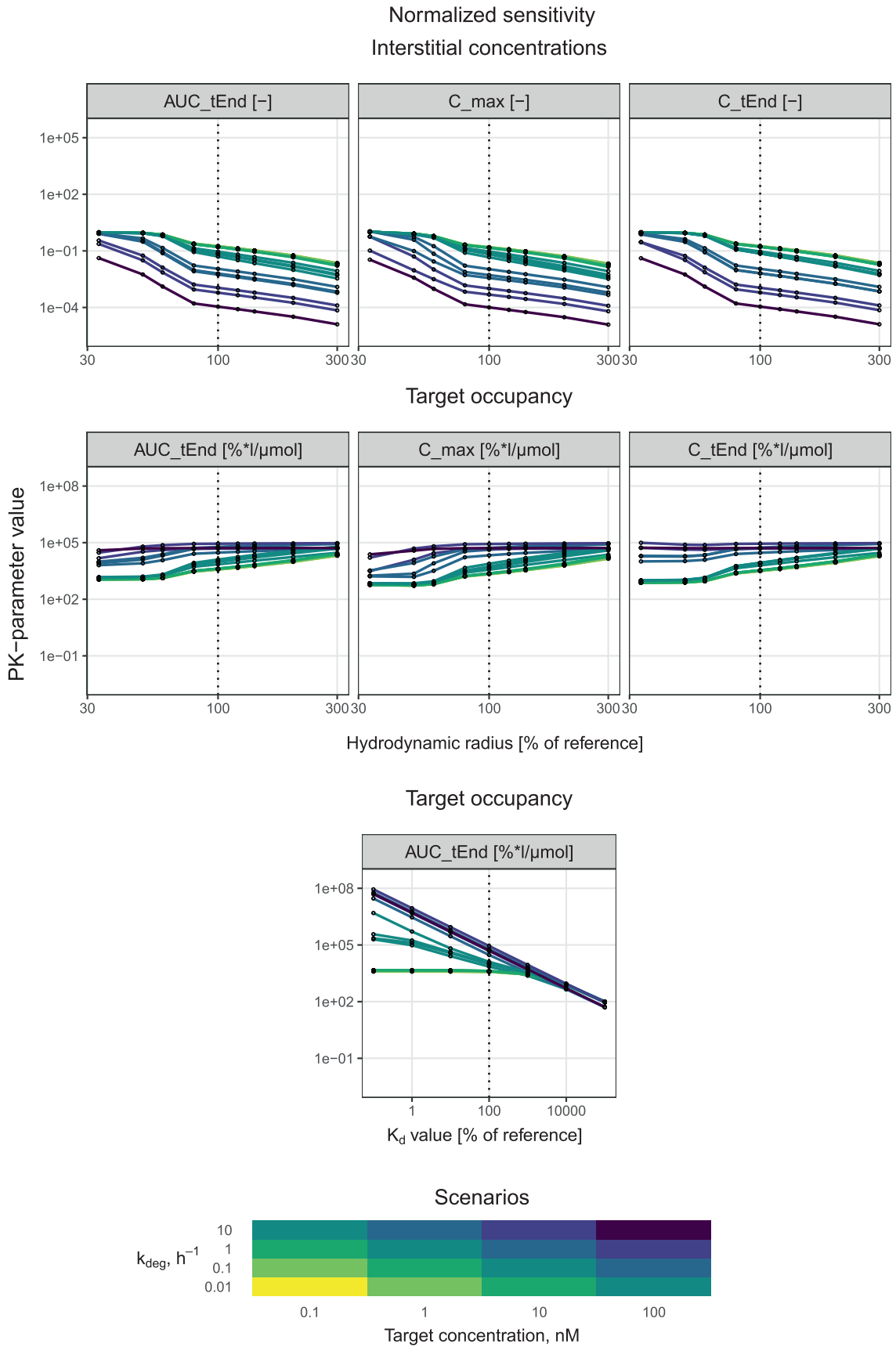

FIGURE 6 The impact of drug molecule hydrodynamic radius on interstitial concentration normalized for plasma concentration and on target occupancy normalized for interstitial concentration, as well as the impact of K_d on target occupancy normalized for interstitial concentration when the target is expressed in the heart.

side of the sensitivity analysis for K_d, it appears that this is mainly due to a change in the K_{ss}, as explained above.

The main insights revealed by the sensitivity analysis are that a whole-body PBPK model with TMDD in tissues behaves very similarly to the minimal TMDD models that are most often applied, with the addition of the potential rate-limiting tissue distribution for large molecules.

Integrating a TMDD and a whole-body PBPK model enabled us to explore relevant scenarios with respect to target binding in any of the major organs or in multiple organs simultaneously in different species and for different molecular sizes of the drug molecule. This is a significant advantage of a whole-body PBPK model in contrast with minimal PBPK models, where the binding organ is often a separate compartment and where binding in multiple organs would require adaptation of the model structure. The reader is encouraged to experience and explore the binding in different organs in our Tissue TMDD shiny app.

Uncertainties

Our review gives a clear indication of the relevance of local TMDD and points toward more attention to target-mediated clearance in tissues, even for drugs with apparently linear pharmacokinetics. A few elements in our analysis require caution when interpreting the results. Firstly, differences between different types of targets and different species in their published parameter values are inconclusive in light of the limited number of data points and the variability within the dataset.

Additionally, biases, which could affect the obtained values, might be present due to other differences between the data from the distinct categories we compared. One example could be the greater ease of measuring plasma concentrations of soluble targets directly compared with membrane targets, which could bias those numbers to lower values for soluble targets. Another example is that the estimation of in vivo target turnover rate constants is almost exclusively provided by estimates from applying TMDD models, which can bias the values to higher rate constants as these values increase the likeliness of nonlinear PK and identifiable TMDD parameters.

Another important remark is the crucial role of the tissue distribution kinetics as predicted by the two-pore model,[14] which limits the tissue distribution of large molecules based on their size, and parameter values in our simulations. This introduces some uncertainty as most of the validations of the two-pore model are derived from tissue distribution studies where the time resolution is often low, and the majority of the data only inform on the extent of the distribution with relatively constant plasma concentrations and less on the kinetics of the tissue distribution. Moreover, our model describes the drug–target interaction in a well-mixed homogeneous interstitial compartment, while especially limited distribution within tissues in combination with TMDD can introduce heterogeneity in the interstitial space. This leads to a well-described phenomenon known as the "Binding Site Barrier" where tumor cells closer to the vascular epithelium get more exposed to antibodies or antibody-drug conjugates compared with more peripheral cells.[92,93] Since this phenomenon has been described mainly for tumors, it might be that the increased colloid pressure in tumors and associated reduced distribution of a drug from plasma to interstitial space contributes to this phenomenon. While the distribution of large molecules to tumors has been successfully reported for the large molecule PK-Sim model,[14] the consequence of their altered distribution kinetics and associated uncertainty was outside the scope of this manuscript.

It is essential to emphasize that our findings are mainly relevant to unsaturated systems, as a target-saturating dose decreases the impact of target-mediated clearance due to a reduction in the fraction of the drug bound to the target in saturating conditions. However, target saturation is more difficult to achieve with strong tissue TMDD due to the local depletion of the drug in the tissues. This is illustrated in Figure 2, where the chosen standard affinity of 1 nM and dose of 1 mg/kg leads to a saturated target in low TMDD conditions but less than 1% occupancy for stronger TMDD conditions. While these uncertainties should be taken into account with respect to the identified parameter value ranges and the values at which local TMDD starts to play a significant role, our central findings remain unaltered.

Our work predicts the tissue interstitial concentrations and target occupancy for many different conditions and hypothetical drugs, and it would take a large and diverse dataset to completely validate our predictions with in vivo data. Such a dataset is not readily available, especially since the validation of our predictions would need either occupancy or interstitial concentration measurements. Since we predict very low interstitial concentrations and occupancy, the required in vivo measurements are difficult to obtain: a standard radiolabeled biodistribution study would not distinguish between vascular and extravascular concentrations, and very low extravascular concentrations would not be precisely identifiable in the sum of very low extravascular and vascular concentrations, which is the measured signal. Moreover, residualizing radiolabels also include the amount degraded in the tissue, and strong TMDD would not lead to lower signals compared with no TMDD, as the

degraded molecules are retained in the signal. Finally, if the target concentration in the tissue is high compared with the tissue concentration of the drug, and the affinity is high, even in the case of strong TMDD and depletion of interstitial concentrations, the decrease in interstitial concentrations will only be observed if measured directly. This can be seen in the lower row of Figure 2, for example, where the target concentration is 100 nM. The green line in this figure ($k_{deg}=0.1\,h^{-1}$) shows an interstitial concentration of <1 nM, tenfold lower than the scenario with the lowest TMDD ($k_{deg}=0.01\,h^{-1}$). However, the occupancy is still ~30%, which gives a target-bound + free interstitial tissue concentration of about 31 nM for this scenario, which would still be observed as "tissue accumulation" as compared with tissues with a concentration of 10 nM, for example. In spite of all of these difficulties, there are still some studies available with advanced measurement methods that (indirectly) support our predictions:

1. The combination of residualizing and non-residualizing radiolabels has shown that the CD3-mediated catabolism in T-cell rich tissues can be significant, and is dependent on the affinity.[94]
2. Intravital microscopy in combination with fluorescently labeled nanobodies and an antibody confirmed the slow and size-dependent extravasation kinetics in mice bearing subcutaneous xenografts.[95]
3. Model-based affinity estimates from in vivo TMDD models without tissue distribution revealed 10–100-fold lower estimates compared with in vitro values, which could potentially be due to the rate-limiting effect of tissue distribution.[96]
4. Application of microdialysis for large molecules revealed moderate dose-dependent interstitial tumor concentration depletion in tumor-bearing mice.[97]
5. The well-described "Binding Site Barrier" phenomenon clearly points to the potential of rate-limiting distribution to interstitial space in combination with target binding to the extent that spatial differences occur within tumor interstitial space, although this phenomenon has been described mainly for tumors.[92,93]

When examining the pharmacokinetic properties of a drug molecule, most attention is typically paid to the concentration of the drug in blood plasma. Results of our study demonstrate that this approach may be inappropriate when the drug–target complex is formed in tissue and not in plasma since the plasma concentration profile may not adequately reflect local drug concentrations. We find the occurrence of local drug depletion a likely condition in the range of physiological parameter values we identified from the literature. Overlooking this aspect can lead to the development of incorrect recommendations for drug dosing and influence the ultimate effectiveness of treatment.

CONCLUSION

This review revealed that TMDD parameters such as target concentration and target turnover have limited variability, and their reference ranges could be established from the available literature. Within the established reference ranges, we found that these parameters are likely to impact the local large molecule drug concentration extensively when a membrane target is expressed in tissue. The simulated TMDD in tissues led to the local depletion of the drug in most scenarios. These findings emphasize the necessity to consider the drug's tissue concentration in these cases, even if the plasma concentration profile does not exhibit nonlinear pharmacokinetics.

Additionally, our simulations and sensitivity analysis demonstrated that the distribution of a drug molecule from plasma to the tissue interstitial space is likely to become the rate-limiting step on the causal path from drug administration to target-mediated elimination, particularly for smaller or less perfused organs. Such scenarios influence the impact of drug–target affinity and the hydrodynamic radius of large molecules and should be taken into account in the design, development, and application of large molecules.

By implementing TMDD in a whole-body PBPK model, we can investigate various scenarios with drug–target binding in any major organ or in multiple organs simultaneously in different species and for compounds with different molecular sizes. This flexibility of a whole-body PBPK modeling with TMDD makes it a beneficial and convenient tool for exploring drug–target interaction in tissue interstitial space.

AUTHOR CONTRIBUTIONS

All authors wrote the manuscript. E.L. and W.W. designed the research. T.Z. and S.S. performed the research. All authors analyzed the data.

ACKNOWLEDGMENTS

We would like to express our gratitude to Felix Mil from ESQlabs GmbH, Saterland, Germany, for developing the Tissue TMDD shiny app.

FUNDING INFORMATION

No funding was received for this work.

CONFLICT OF INTEREST STATEMENT

The opinions expressed in the manuscript are those of the authors and should not be interpreted as the position of their organizations/employers. T.Z., S.S., and W.E.A.W. are full-time employees of ESQlabs GmbH and may hold stock or options. The authors declared no competing interests for this work.

ORCID

Tatiana Zasedateleva https://orcid.org/0009-0008-7415-7269
Stephan Schaller https://orcid.org/0000-0003-1046-7651
Elizabeth C. M. de Lange https://orcid.org/0000-0001-8303-1117
Wilhelmus E. A. de Witte https://orcid.org/0000-0002-0840-3619

REFERENCES

1. Levy G. Pharmacologic target-mediated drug disposition. *Clin Pharmacol Ther*. 1994;56(3):248-252. doi:10.1038/clpt.1994.134
2. Dua P, Hawkins E, van der Graaf P. A tutorial on target-mediated drug disposition (TMDD) models. *CPT Pharmacometrics Syst Pharmacol*. 2015;4(6):324-337. doi:10.1002/psp4.41
3. An G. Concept of pharmacologic target-mediated drug disposition (TMDD) in large-molecule and small-molecule compounds. *J Clin Pharmacol*. 2020;60(2):149-163. doi:10.1002/jcph.1545
4. Peletier LA, Gabrielsson J. Dynamics of target-mediated drug disposition: characteristic profiles and parameter identification. *J Pharmacokinet Pharmacodyn*. 2012;39(5):429-451. doi:10.1007/s10928-012-9260-6
5. Mager DE, Jusko WJ. General pharmacokinetic model for drugs exhibiting target-mediated drug disposition. *J Pharmacokinet Pharmacodyn*. 2001;28(6):507-532. doi:10.1023/A:1014414520282
6. Ryman JT, Meibohm B. Pharmacokinetics of monoclonal antibodies. *CPT Pharmacometrics Syst Pharmacol*. 2017;6(9):576-588. doi:10.1002/psp4.12224
7. Liu L. Pharmacokinetics of monoclonal antibodies and fc-fusion proteins. *Protein Cell*. 2018;9(1):15-32. doi:10.1007/s13238-017-0408-4
8. Tang Y, Cao Y. Modeling pharmacokinetics and pharmacodynamics of therapeutic antibodies: progress, challenges, and future directions. *Pharmaceutics*. 2021;13(3):422. doi:10.3390/pharmaceutics13030422
9. Gabrielsson J, Peletier LA. Pharmacokinetic steady-states highlight interesting target-mediated disposition properties. *AAPS J*. 2017;19(3):772-786. doi:10.1208/s12248-016-0031-y
10. Cao Y, Jusko WJ. Incorporating target-mediated drug disposition in a minimal physiologically-based pharmacokinetic model for monoclonal antibodies. *J Pharmacokinet Pharmacodyn*. 2014;41(4):375-387. doi:10.1007/s10928-014-9372-2
11. Grimm HP. Gaining insights into the consequences of target-mediated drug disposition of monoclonal antibodies using quasi-steady-state approximations. *J Pharmacokinet Pharmacodyn*. 2009;36(5):407-420. doi:10.1007/s10928-009-9129-5
12. Spilker ME, Singh P, Vicini P. Mathematical modeling of receptor occupancy data: a valuable technology for biotherapeutic drug development. *Cytometry B Clin Cytom*. 2016;90(2):230-236. doi:10.1002/cyto.b.21318
13. Willmann S, Lippert J, Sevestre M, Solodenko J, Fois F, Schmitt W. PK-Sim®: a physiologically based pharmacokinetic 'whole-body' model. *Biosilico*. 2003;1(4):121-124. doi:10.1016/S1478-5382(03)02342-4
14. Niederalt C, Kuepfer L, Solodenko J, et al. A generic whole body physiologically based pharmacokinetic model for therapeutic proteins in PK-Sim. *J Pharmacokinet Pharmacodyn*. 2018;45(2):235-257. doi:10.1007/s10928-017-9559-4
15. Millet P, Ibáñez V, Delforge J, Pappata S, Guimón J. Wavelet analysis of dynamic PET data: application to the parametric imaging of benzodiazepine receptor concentration. *NeuroImage*. 2000;11(5):458-472. doi:10.1006/nimg.2000.0563
16. Millet P, Graf C, Moulin M, Ibanez V. SPECT quantification of benzodiazepine receptor concentration using a dual-ligand approach. *J Nucl Med*. 2006;47:783-792.
17. Costes N, Merlet I, Zimmer L, et al. Modeling [18F]MPPF positron emission tomography kinetics for the determination of 5-Hydroxytryptamine(1A) receptor concentration with multisection. *J Cereb Blood Flow Metab*. 2002;22:753-765. doi:10.1097/00004647-200206000-00014
18. Wooten D, Hillmer A, Moirano J, et al. Measurement of 5-HT1A receptor density and in-vivo binding parameters of [18F] mefway in the nonhuman primate. *J Cereb Blood Flow Metab*. 2012;32:1546-1558. doi:10.1038/jcbfm.2012.43
19. Le Guludec D, Cohen-Solal A, Delforge J, Delahaye N, Syrota A, Merlet P. Increased myocardial muscarinic receptor density in idiopathic dilated cardiomyopathy. *Circulation*. 1997;96:3416-3422. doi:10.1161/01.cir.96.10.3416
20. Delahaye N, Le Guludec D, Dinanian S, et al. Myocardial muscarinic receptor upregulation and normal response to isoproterenol in denervated hearts by familial amyloid polyneuropathy. *Circulation*. 2001;104:2911-2916. doi:10.1161/hc4901.100380
21. Hietala J, Nagren K, Lehikoinen P, Ruotsalainen U, Syvalahti E. Measurement of striatal D2 dopamine receptor density and affinity with [11C]-raclopride in vivo: a test-retest analysis. *J Cereb Blood Flow Metab*. 1999;19:210-217. doi:10.1097/00004647-199902000-00012
22. Delforge J, Bottlaender M, Loc'h C, Dolle F, Syrota A. Parametric images of the extrastriatal D2 receptor density obtained using a high-affinity ligand (FLB 457) and a double-saturation method. *J Cereb Blood Flow Metab*. 2001;21(12):1493-1503. doi:10.1097/00004647-200112000-00014
23. Delforge J, Bottlaender M, Loc'h C, et al. Quantitation of Extrastriatal D2 receptors using a very high-affinity ligand (FLB 457) and the multi-injection approach. *J Cereb Blood Flow Metab*. 1999;19:533-546. doi:10.1097/00004647-199905000-00008
24. Delforge J, Mesangeau D, Dolle F, et al. In vivo quantification and parametric images of the cardiac β-adrenergic receptor density. *J Nucl Med*. 2002;43(2):215-226.
25. Lefroy DC, de Silva R, Choudhury L, et al. Diffuse reduction of myocardial beta-adrenoceptors in hypertrophic cardiomyopathy: a study with positron emission tomography. *J Am Coll Cardiol*. 1993;22(6):1653-1660. doi:10.1016/0735-1097(93)90591-N
26. Merlet P, Delforge J, Syrota A, et al. Positron emission tomography with 11C CGP-12177 to assess beta-adrenergic receptor concentration in idiopathic dilated cardiomyopathy. *Circulation*. 1993;87(4):1169-1178. doi:10.1161/01.CIR.87.4.1169

27. Delforge J, Syrota A, Lançon JP, et al. Cardiac beta-adrenergic receptor density measured in vivo using PET, CGP 12177, and a new graphical method. *J Nucl Med*. 1991;32(4):739-748.
28. Gallezot JD, Bottlaender MA, Delforge J, et al. Quantification of cerebral nicotinic acetylcholine receptors by PET using 2-[18F]Fluoro-A-85380 and the multiinjection approach. *J Cereb Blood Flow Metab*. 2008;28(1):172-189. doi:10.1038/sj.jcbfm.9600505
29. Hillmer AT, Wooten DW, Slesarev MS, et al. Measuring α4β2* nicotinic acetylcholine receptor density in vivo with [18F] nifene PET in the nonhuman primate. *J Cereb Blood Flow Metab*. 2013;33(11):1806-1814. doi:10.1038/jcbfm.2013.136
30. Tomasi G, Nabulsi N, Zheng MQ, et al. Determination of in vivo B_{max} and K_d for [11C]GR103545, an agonist PET tracer for kappa opioid receptors: a study in nonhuman primates. *J Nucl Med off Publ Soc Nucl Med*. 2013;54(4):600-608. doi:10.2967/jnumed.112.112672
31. Vivash L, Gregoire MC, Bouilleret V, et al. In vivo measurement of hippocampal GABAA/cBZR density with [18F]-flumazenil PET for the study of disease progression in an animal model of temporal lobe epilepsy. *PLoS One*. 2014;9(1):e86722. doi:10.1371/journal.pone.0086722
32. Yanamoto K, Kumata K, Fujinaga M, et al. In vivo imaging and quantitative analysis of TSPO in rat peripheral tissues using small-animal PET with [18F]FEDAC. *Nucl Med Biol*. 2010;37(7):853-860. doi:10.1016/j.nucmedbio.2010.04.183
33. Yamasaki T, Fujinaga M, Kawamura K, et al. In vivo measurement of the affinity and density of metabotropic glutamate receptor subtype 1 in rat brain using 18F-FITM in small-animal PET. *J Nucl Med*. 2012;53(10):1601-1607. doi:10.2967/jnumed.112.105908
34. Valette H, Dollé F, Guenther I, et al. In vivo quantification of myocardial Dihydropyridine binding sites: a PET study in dogs. *J Nucl Med*. 2002;43(9):1227-1233.
35. Xia Y, Zheng MQ, Holden D, et al. Measurement of B_{max} and K_d with the glycine transporter 1 radiotracer 18F-MK6577 using a novel multi-infusion paradigm. *J Cereb Blood Flow Metab*. 2015;35(12):2001-2009. doi:10.1038/jcbfm.2015.163
36. Bottlaender M, Valette H, Delforge J, et al. In vivo quantification of monoamine oxidase a in baboon brain: a PET study using [11C]befloxatone and the multi-injection approach. *J Cereb Blood Flow Metab*. 2010;30(4):792-800. doi:10.1038/jcbfm.2009.242
37. Chen T, Mager DE, Kagan L. Interspecies modeling and prediction of human exenatide pharmacokinetics. *Pharm Res*. 2013;30(3):751-760. doi:10.1007/s11095-012-0917-z
38. Li H, Xu J, Fan X. Target-mediated pharmacokinetic/pharmacodynamic model based meta-analysis and dosing regimen optimization of a long-acting release formulation of exenatide in patients with type 2 diabetes mellitus. *J Pharmacol Sci*. 2015;127(2):170-180. doi:10.1016/j.jphs.2014.12.004
39. Kagan L, Abraham AK, Harrold JM, Mager DE. Interspecies scaling of receptor-mediated pharmacokinetics and pharmacodynamics of type I interferons. *Pharm Res*. 2010;27(5):920-932. doi:10.1007/s11095-010-0098-6
40. Le KN, Gibiansky L, Good J, et al. A mechanistic pharmacokinetic/Pharmacodynamic model of factor D inhibition in Cynomolgus monkeys by Lampalizumab for the treatment of geographic atrophy. *J Pharmacol Exp Ther*. 2015;355(2):288-296. doi:10.1124/jpet.115.227223
41. Marathe A, Peterson MC, Mager DE. Integrated cellular bone homeostasis model for denosumab pharmacodynamics in multiple myeloma patients. *J Pharmacol Exp Ther*. 2008;326(2):555-562. doi:10.1124/jpet.108.137703
42. Parra-Guillen ZP, Janda A, Alzuguren P, Berraondo P, Hernandez-Alcoceba R, Troconiz IF. Target-mediated disposition model describing the dynamics of IL12 and IFNγ after administration of a mifepristone-inducible adenoviral vector for IL-12 expression in mice. *AAPS J*. 2012;15(1):183-194. doi:10.1208/s12248-012-9423-9
43. Woo S, Krzyzanski W, Jusko WJ. Target-mediated pharmacokinetic and pharmacodynamic model of recombinant human erythropoietin (rHuEPO). *J Pharmacokinet Pharmacodyn*. 2007;34(6):849-868. doi:10.1007/s10928-007-9074-0
44. Brodfuehrer J, Rankin A, Edmonds J, et al. Quantitative analysis of target coverage and germinal center response by a CXCL13 neutralizing antibody in a T-dependent mouse immunization model. *Pharm Res*. 2014;31(3):635-648. doi:10.1007/s11095-013-1185-2
45. Li H, Köck K, Wisler JA, et al. Prediction of clinical pharmacokinetics of AMG 181, a human anti-α4β7 monoclonal antibody for treating inflammatory bowel diseases. *Pharmacol Res Perspect*. 2015;3(1):e00098. doi:10.1002/prp2.98
46. Liu X, Ou YC, Zhang J, et al. Pharmacokinetics and pharmacodynamics of CD4-anchoring bi-functional fusion inhibitor in monkeys. *Pharm Res*. 2014;31(3):809-818. doi:10.1007/s11095-013-1203-4
47. Mager DE, Krzyzanski W. Quasi-equilibrium pharmacokinetic model for drugs exhibiting target-mediated drug disposition. *Pharm Res*. 2005;22(10):1589-1596. doi:10.1007/s11095-005-6650-0
48. Vugmeyster Y, Rohde C, Perreault M, Gimeno RE, Singh P. Agonistic TAM-163 antibody targeting tyrosine kinase receptor-B. *MAbs*. 2013;5(3):373-383. doi:10.4161/mabs.23826
49. Zhang L, Mager DE. Physiologically-based pharmacokinetic modeling of target-mediated drug disposition of Bortezomib in mice. *J Pharmacokinet Pharmacodyn*. 2015;42(5):541-552. doi:10.1007/s10928-015-9445-x
50. Djebli N, Martinez JM, Lohan L, et al. Target-mediated drug disposition population pharmacokinetics model of Alirocumab in healthy volunteers and patients: pooled analysis of randomized phase I/II/III studies. *Clin Pharmacokinet*. 2017;56(10):1155-1171. doi:10.1007/s40262-016-0505-1
51. Berends SE, van Steeg TJ, Ahsman MJ, et al. Tumor necrosis factor-mediated disposition of infliximab in ulcerative colitis patients. *J Pharmacokinet Pharmacodyn*. 2019;46(6):543-551. doi:10.1007/s10928-019-09652-5
52. Wong DF, Kuwabara H, Horti AG, et al. Brain PET imaging of α7-nAChR with [18F]ASEM: reproducibility, occupancy, receptor density, and changes in schizophrenia. *Int J Neuropsychopharmacol*. 2018;21(7):656-667. doi:10.1093/ijnp/pyy021
53. Nabulsi NB, Mercier J, Holden D, et al. Synthesis and preclinical evaluation of 11C-UCB-J as a PET tracer for imaging the synaptic vesicle glycoprotein 2A in the brain. *J Nucl Med*. 2016;57(5):777-784. doi:10.2967/jnumed.115.168179
54. Wiczling P, Lowe P, Pigeolet E, Lüdicke F, Balser S, Krzyzanski W. Population pharmacokinetic modelling of Filgrastim in healthy adults following intravenous and subcutaneous administrations. *Clin Pharmacokinet*. 2009;48(12):817-826. doi:10.2165/11318090-000000000-00000

55. Wei X, Gibiansky L, Wang Y, et al. Pharmacokinetic and pharmacodynamic modeling of serum etrolizumab and circulating β7 receptor occupancy in patients with ulcerative colitis. *J Clin Pharmacol*. 2018;58(3):386-398. doi:10.1002/jcph.1031
56. Chen P, Vu T, Narayanan A, et al. Pharmacokinetic and pharmacodynamic relationship of AMG 811, an anti-IFN-γ IgG1 monoclonal antibody, in patients with systemic lupus erythematosus. *Pharm Res*. 2015;32(2):640-653. doi:10.1007/s11095-014-1492-2
57. Yoshida K, Moein A, Bittner T, et al. Pharmacokinetics and pharmacodynamic effect of crenezumab on plasma and cerebrospinal fluid beta-amyloid in patients with mild-to-moderate Alzheimer's disease. *Alzheimers Res Ther*. 2020;12:16. doi:10.1186/s13195-020-0580-2
58. Ahlberg J, Giragossian C, Li H, et al. Retrospective analysis of model-based predictivity of human pharmacokinetics for anti-IL-36R monoclonal antibody MAB92 using a rat anti-mouse IL-36R monoclonal antibody and RNA expression data (FANTOM5). *MAbs*. 2019;11(5):956-964. doi:10.1080/19420862.2019.1615345
59. Chen X, Jiang X, Jusko WJ, Zhou H, Wang W. Minimal physiologically-based pharmacokinetic (mPBPK) model for a monoclonal antibody against interleukin-6 in mice with collagen-induced arthritis. *J Pharmacokinet Pharmacodyn*. 2016;43(3):291-304. doi:10.1007/s10928-016-9472-2
60. Bon C, Hofer T, Bousquet-Mélou A, Davies MR, Krippendorff BF. Capacity limits of asialoglycoprotein receptor-mediated liver targeting. *MAbs*. 2017;9(8):1360-1369. doi:10.1080/19420862.2017.1373924
61. Betts A, Clark T, Jasper P, et al. Use of translational modeling and simulation for quantitative comparison of PF-06804103, a new generation HER2 ADC, with trastuzumab-DM1. *J Pharmacokinet Pharmacodyn*. 2020;47(5):513-526. doi:10.1007/s10928-020-09702-3
62. Ternant D, Le Tilly O, Picon L, et al. Infliximab efficacy May Be linked to full TNF-α blockade in peripheral compartment—a double central-peripheral target-mediated drug disposition (TMDD) model. *Pharmaceutics*. 2021;13(11):1821. doi:10.3390/pharmaceutics13111821
63. Tiwari A, Kasaian M, Heatherington AC, Jones HM, Hua F. A mechanistic PK/PD model for two anti-IL13 antibodies explains the difference in total IL-13 accumulation observed in clinical studies. *MAbs*. 2016;8(5):983-990. doi:10.1080/19420862.2016.1172151
64. Olsson H, Halldin C, Farde L. Differentiation of extrastriatal dopamine D2 receptor density and affinity in the human brain using PET. *NeuroImage*. 2004;22(2):794-803. doi:10.1016/j.neuroimage.2004.02.002
65. Karlsson P, Farde L, Halldin C, Sedvall G. PET study of D1 dopamine receptor binding in neuroleptic-naive patients with schizophrenia. *Am J Psychiatry*. 2002;159(5):761-767. doi:10.1176/appi.ajp.159.5.761
66. Doze P, Elsinga PH, van Waarde A, et al. Quantification of β-adrenoceptor density in the human heart with (S)-[11C]CGP 12388 and a tracer kinetic model. *Eur J Nucl Med Mol Imaging*. 2002;29(3):295-304. doi:10.1007/s00259-001-0714-0
67. Itoh T, Abe K, Zoghbi SS, et al. PET measurement of the in vivo affinity of 11C-(R)-rolipram and the density of its target, phosphodiesterase-4, in the brains of conscious and anesthetized rats. *J Nucl Med Off Publ Soc Nucl Med*. 2009;50(5):749-756. doi:10.2967/jnumed.108.058305
68. Valette H, Bottlaender M, Dollé F, Coulon C, Ottaviani M, Syrota A. Acute inhibition of cardiac monoamine oxidase a after tobacco smoke inhalation: validation study of [11C] Befloxatone in rats followed by a positron emission tomography application in baboons. *J Pharmacol Exp Ther*. 2005;314(1):431-436. doi:10.1124/jpet.105.085704
69. Sossi V, Holden JE, Topping GJ, et al. In vivo measurement of density and affinity of the monoamine vesicular transporter in a unilateral 6-hydroxydopamine rat model of PD. *J Cereb Blood Flow Metab*. 2007;27(7):1407-1415. doi:10.1038/sj.jcbfm.9600446
70. Laruelle M, Abi-Dargham A, AI-Tikriti MS, et al. SPECT quantification of [123I]Iomazenil binding to benzodiazepine receptors in nonhuman primates: II. Equilibrium analysis of constant infusion experiments and correlation with in vitro parameters. *J Cereb Blood Flow Metab*. 1994;14(3):453-465. doi:10.1038/jcbfm.1994.56
71. Narendran R, Hwang DR, Slifstein M, et al. Measurement of the proportion of D2 receptors configured in state of high affinity for agonists in vivo: a positron emission tomography study using [11C]N-propyl-norapomorphine and [11C]Raclopride in baboons. *J Pharmacol Exp Ther*. 2005;315(1):80-90. doi:10.1124/jpet.105.090068
72. Roy J, Warner BM, Basuli F, et al. Comparison of prostate-specific membrane antigen expression levels in human salivary glands to non-human primates and rodents. *Cancer Biother Radiopharm*. 2020;35(4):284-291. doi:10.1089/cbr.2019.3079
73. Ait-Oudhia S, Scherrmann JM, Krzyzanski W. Simultaneous pharmacokinetics/pharmacodynamics modeling of recombinant human erythropoietin upon multiple intravenous dosing in rats. *J Pharmacol Exp Ther*. 2010;334(3):897-910. doi:10.1124/jpet.110.167304
74. Gao W, Jusko WJ. Pharmacokinetic and pharmacodynamic modeling of exendin-4 in type 2 diabetic Goto-Kakizaki rats. *J Pharmacol Exp Ther*. 2011;336(3):881-890. doi:10.1124/jpet.110.175752
75. Cai W, Leil TA, Gibiansky L, et al. Modeling and simulation of the pharmacokinetics and target engagement of an antagonist monoclonal antibody to interferon-γ–induced protein 10, BMS-986184, in healthy participants to guide therapeutic dosing. *Clin Pharmacol Drug Dev*. 2020;9(6):689-698. doi:10.1002/cpdd.784
76. Conner KP, Pastuskovas CV, Soto M, Thomas VA, Wagner M, Rock DA. Preclinical characterization of the ADME properties of a surrogate anti-IL-36R monoclonal antibody antagonist in mouse serum and tissues. *MAbs*. 2020;12(1):1746520. doi:10.1080/19420862.2020.1746520
77. Krzyzanski W, Wyska E. Pharmacokinetics and pharmacodynamics of erythropoietin receptor in healthy volunteers. *Naunyn Schmiedeberg's Arch Pharmacol*. 2008;377(4–6):637-645. doi:10.1007/s00210-007-0225-z
78. El-Komy MH, Widness JA, Veng-Pedersen P. Pharmacokinetic analysis of continuous erythropoietin receptor activator disposition in adult sheep using a target-mediated, physiologic recirculation model and a tracer interaction methodology. *Drug Metab Dispos*. 2011;39(4):603-609. doi:10.1124/dmd.110.036236
79. Hazra A, DuBois DC, Almon RR, Jusko WJ. Assessing the dynamics of nuclear glucocorticoid-receptor complex: adding flexibility to gene expression modeling. *J Pharmacokinet Pharmacodyn*. 2007;34(3):333-354. doi:10.1007/s10928-007-9049-1

80. Betts AM, Clark TH, Yang J, et al. The application of target information and preclinical pharmacokinetic/Pharmacodynamic modeling in predicting clinical doses of a Dickkopf-1 antibody for osteoporosis. *J Pharmacol Exp Ther*. 2010;333(1):2-13. doi:10.1124/jpet.109.164129
81. Ng CM, Stefanich E, Anand BS, Fielder PJ, Vaickus L. Pharmacokinetics/pharmacodynamics of nondepleting anti-CD4 monoclonal antibody (TRX1) in healthy human volunteers. *Pharm Res*. 2006;23(1):95-103. doi:10.1007/s11095-005-8814-3
82. Vu T, Ma P, Chen JS, et al. Pharmacokinetic-pharmacodynamic relationship of Erenumab (AMG 334) and capsaicin-induced dermal blood flow in healthy and migraine subjects. *Pharm Res*. 2017;34(9):1784-1795. doi:10.1007/s11095-017-2183-6
83. Pawaskar D, Chen X, Glassman F, et al. Pharmacokinetic/pharmacodynamic modeling for dose selection for the first-in-human trial of the activated factor XII inhibitor garadacimab (CSL312). *Clin Transl Sci*. 2022;15(3):709-720. doi:10.1111/cts.13192
84. Abraham AK, Kagan L, Kumar S, Mager DE. Type I interferon receptor is a primary regulator of target-mediated drug disposition of interferon-β in mice. *J Pharmacol Exp Ther*. 2010;334(1):327-332. doi:10.1124/jpet.110.167650
85. Wang B, Lau YY, Liang M, et al. Mechanistic modeling of antigen sink effect for mavrilimumab following intravenous Administration in Patients with Rheumatoid Arthritis. *J Clin Pharmacol*. 2012;52(8):1150-1161. doi:10.1177/0091270011412964
86. Kakkar T, Sung C, Gibiansky L, et al. Population PK and IgE pharmacodynamic analysis of a fully human monoclonal antibody against IL4 receptor. *Pharm Res*. 2011;28(10):2530-2542. doi:10.1007/s11095-011-0481-y
87. Wang YMC, Krzyzanski W, Doshi S, Xiao JJ, Pérez-Ruixo JJ, Chow AT. Pharmacodynamics-mediated drug disposition (PDMDD) and precursor pool lifespan model for single dose of Romiplostim in healthy subjects. *AAPS J*. 2010;12(4):729-740. doi:10.1208/s12248-010-9234-9
88. Kato Y, Sato H, Ichikawa M, et al. Existence of two pathways for the endocytosis of epidermal growth factor by rat liver: phenylarsine oxide-sensitive and -insensitive pathways. *Proc Natl Acad Sci USA*. 1992;89(18):8507-8511. doi:10.1073/pnas.89.18.8507
89. Vainshtein I, Roskos LK, Cheng J, Sleeman MA, Wang B, Liang M. Quantitative measurement of the target-mediated internalization kinetics of biopharmaceuticals. *Pharm Res*. 2015;32(1):286-299. doi:10.1007/s11095-014-1462-8
90. Trincavelli ML, Tuscano D, Cecchetti P, et al. Agonist-induced internalization and recycling of the human A3 adenosine receptors. *J Neurochem*. 2000;75(4):1493-1501. doi:10.1046/j.1471-4159.2000.0751493.x
91. Tanaka T, Fujishima Y, Kaneo Y. Receptor mediated endocytosis and cytotoxicity of transferrin-Mitomycin C conjugate in the HepG2 cell and primary cultured rat hepatocyte. *Biol Pharm Bull*. 2001;24(3):268-273. doi:10.1248/bpb.24.268
92. Juweid M, Neumann R, Paik C, et al. Micropharmacology of monoclonal antibodies in solid tumors: direct experimental evidence for a binding site barrier. *Cancer Res*. 1992;52(19):5144-5153.
93. Chen P, Bordeau BM, Zhang Y, Balthasar JP. Transient inhibition of Trastuzumab–tumor binding to overcome the "binding-site barrier" and improve the efficacy of a Trastuzumab–Gelonin immunotoxin. *Mol Cancer Ther*. 2022;21(10):1573-1582. doi:10.1158/1535-7163.MCT-22-0192
94. Mandikian D, Takahashi N, Lo AA, et al. Relative target affinities of T-cell-dependent bispecific antibodies determine biodistribution in a solid tumor mouse model. *Mol Cancer Ther*. 2018;17(4):776-785. doi:10.1158/1535-7163.MCT-17-0657
95. Debie P, Lafont C, Defrise M, et al. Size and affinity kinetics of nanobodies influence targeting and penetration of solid tumours. *J Control Release*. 2020;317:34-42. doi:10.1016/j.jconrel.2019.11.014
96. Singh AP, Krzyzanski W, Martin SW, et al. Quantitative prediction of human pharmacokinetics for mAbs exhibiting target-mediated disposition. *AAPS J*. 2014;17(2):389-399. doi:10.1208/s12248-014-9690-8
97. Khaowroongrueng V, Jadhav SB, Syed M, et al. Pharmacokinetics and determination of tumor interstitial distribution of a therapeutic monoclonal antibody using large-pore microdialysis. *J Pharm Sci*. 2021;110(8):3061-3068. doi:10.1016/j.xphs.2021.03.022

SUPPORTING INFORMATION

Additional supporting information can be found online in the Supporting Information section at the end of this article.

How to cite this article: Zasedateleva T, Schaller S, de Lange ECM, de Witte WEA. Local depletion of large molecule drugs due to target binding in tissue interstitial space. *CPT Pharmacometrics Syst Pharmacol*. 2024;13:2068-2086. doi:10.1002/psp4.13262